Available online at www.sciencedirect.com

SCIENCE DIRECT®

Tectonophysics 400 (2005) 127–151

TECTONOPHYSICS

www.elsevier.com/locate/tecto

Low temperature Phanerozoic history of the Northern Yilgarn Craton, Western Australia

U.D. Weber[a,*], B.P. Kohn[a], A.J.W. Gleadow[a], D.R. Nelson[b]

[a]*School of Earth Sciences, The University of Melbourne, Victoria 3010, Australia*
[b]*Geological Survey of Western Australia, 100 Plain Street, East Perth, WA, 6004, and Department of Applied Physics, Curtin University of Technology, Perth, WA 6001, Australia*

Received 5 April 2004; accepted 1 March 2005
Available online 8 April 2005

Abstract

The Phanerozoic cooling history of the Western Australian Shield has been investigated using apatite fission track (AFT) thermochronology. AFT ages from the northern part of the Archaean Yilgarn Craton, Western Australia, primarily range between 200 and 280 Ma, with mean confined horizontal track lengths varying between 11.5 and 14.3 μm. Time–temperature modelling of the AFT data together with geological information suggest the onset of a regional cooling episode in the Late Carboniferous/Early Permian, which continued into Late Jurassic/Early Cretaceous time. Present-day heat flow measurements on the Western Australian Shield fall in the range of 40–50 mW m^{-2}. If the present day geothermal gradient of $\sim 18 \pm 2$ °C km^{-1} is representative of average Phanerozoic gradients, then this implies a minimum of ~50 °C of Late Palaeozoic to Mesozoic cooling. Assuming that cooling resulted from denudation, the data suggest the removal of at least 3 km of rock section from the northern Yilgarn Craton over this interval. The Perth Basin, located west of the Yilgarn Craton, contains up to 15 km of mostly Permian to Lower Cretaceous clastic sediment. However, published U–Pb data of detrital zircons from Permian and Lower Triassic basin strata show relatively few or no grains of Archaean age. This suggests that the recorded cooling can probably be attributed to the removal of a sedimentary cover rather than by denudation of material from the underlying craton itself. The onset of cooling is linked to tectonism related to either the waning stages of the Alice Springs Orogeny or to the early stages of Gondwana breakup.

Keywords: Apatite; Fission track dating; Thermochronology; Denudation; Tectonics; Yilgarn Craton; Western Australia; Gondwanaland; Supercontinents

1. Introduction

The antiquity of rocks in the Western Australia shield combined with its relatively subdued topography has led to the notion that this continental

* Corresponding author.
E-mail addresses: udweber@unimelb.edu.au (U.D. Weber), b.kohn@unimelb.edu.au (B.P. Kohn).

0040-1951/$ - see front matter © 2005 Elsevier B.V. All rights reserved.
doi:10.1016/j.tecto.2005.03.008

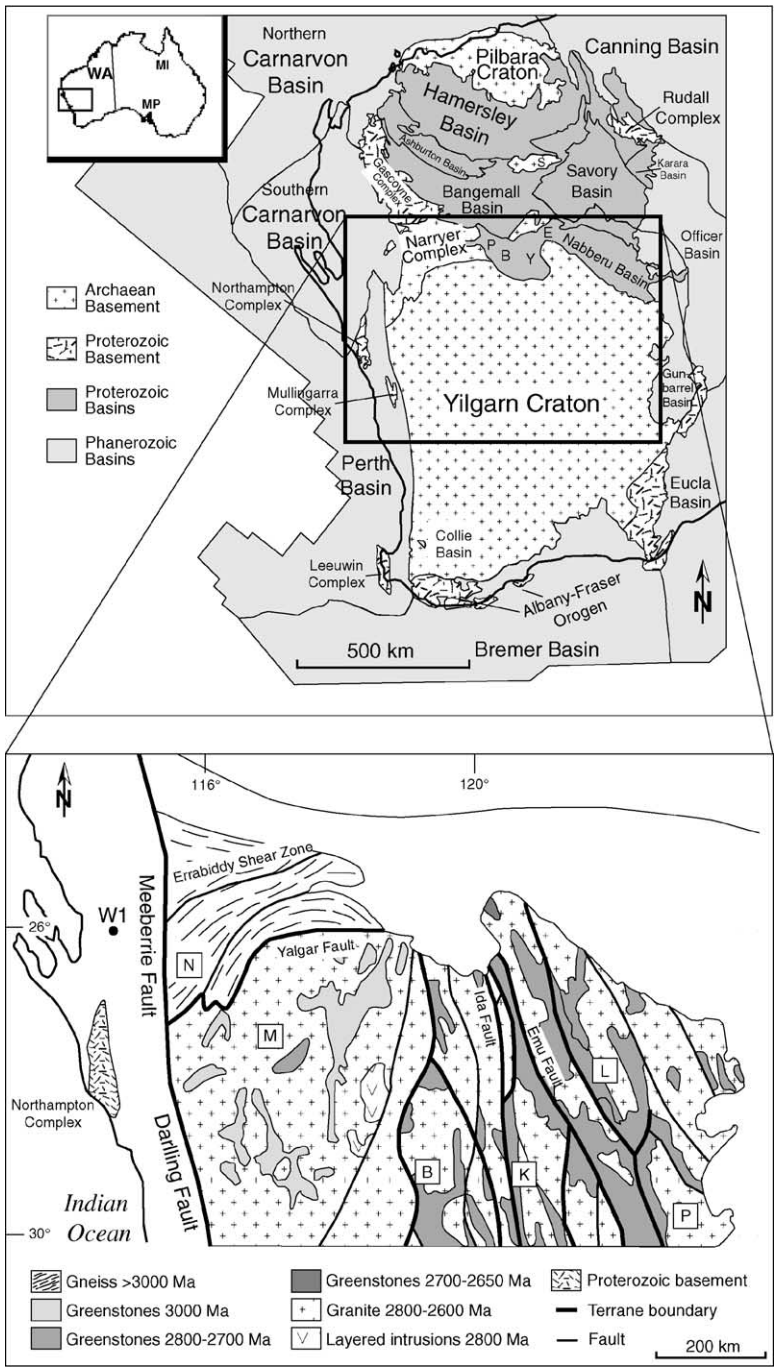

Fig. 1. Upper map: Location of study area (box) and regional geology. MI=Mount Isa, MP=Mount Painter, WA=Western Australia State; Proterozoic basins: B=Bryah, E=Earaheedy, P=Padbury, Y=Yerrida. Lower map: Tectonic terranes with rock types and their age relationships comprising the northern Yilgarn Craton (modified after Myers, 1993; Wilde et al., 1996). Terranes: B=Barlee, K=Kalgoorlie, L=Laverton, M=Murchison, N=Narryer, P=Pinjin. W1=Woodleigh1 well location.

nucleus has remained relatively stable and has not experienced any major heating or cooling events since Mesoproterozoic time and that the overall flatness may represent a Proterozoic erosion surface (Daniels, 1975; Fairbridge and Finkl, 1980).

The Western Australian Shield is an amalgamation of two Archaean cratons and several Proterozoic basins and terranes, which is surrounded by Phanerozoic basins (Fig. 1). The Yilgarn Craton, to the south, constitutes approximately two-thirds of the shield, whereas the Pilbara Craton, to the north, is considerably smaller. The suture between the cratons is obscured by overlying Proterozoic basins, namely the Hamersley, Ashburton, Bangemall (including Collier and Edmund Subbasins), Savory, Officer, Karara, Padbury, Bryah, Yerrida, Earaheedy and Nabberu Basins (Fig. 1). The Sylvania Inlier is considered to be part of the Pilbara Craton, whereas the Gascoyne and Rudall Complexes consist of crystalline Proterozoic basement. Previous geochronological data from much of the Yilgarn Craton, including SHRIMP U–Pb zircon, Sm–Nd data (e.g. Myers, 1993; Nutman et al., 1993; Nelson et al., 1995; Myers et al., 1996) and ^{40}Ar–^{39}Ar hornblende and muscovite analyses (Wijbrans and McDougall, 1987), constrain the timing of formation and metamorphism to Middle to Late Archaean. The study area also includes the Archaean Narryer Gneiss area (Fig. 1) where the oldest detrital zircons on earth have been dated at ~4.4 Ga (e.g. Wilde et al., 2001). The youngest ages documented from the shield are recorded from the Bangemall Supergroup and range between 1630 Ma to ~1070 Ma (e.g. Martin and Thorne, 2004). Pidgeon and Cook (2003) and Qiu et al. (1999) report ~1210 Ma ages from intrusions in the southwestern and northern central Yilgarn Craton, respectively.

More recently evidence for Neoproterozoic and Early Phanerozoic tectonic activity across the southwestern margin of the Yilgarn Craton has come from Rb–Sr biotite ages (Libby and De Laeter, 1998; Libby et al., 1999) and an AFT study, which suggests a period of significant Late Carboniferous to Mid-Jurassic cooling (e.g. Kohn et al., 2002; Gleadow et al., 2002a).

Global plate tectonic processes, such as the amalgamation of Gondwana and Laurasia, which formed the supercontinent Pangaea during the Alice Springs Orogeny (400–300 Ma) (Dunlap and Teyssier, 1995), and subsequent breakup involved the Western Australian Shield. However, the record of these Phanerozoic events is not readily detectable in the history of the shield because conventional stratigraphic markers or cross-cutting relationships, that might be used for reconstructing the regional structural and tectonic evolution, are largely absent.

In this study we apply apatite fission track (AFT) thermochronology with the aim of evaluating whether the northern part of the Yilgarn Craton has retained a record of tectonic processes and dynamic change or whether it has remained a rigid, relatively stable cratonic block since the post-Mesoproterozoic.

2. Geological framework

To better understand the implications of this study it is necessary to place them within the context of the regional geological history.

2.1. Precambrian

The Yilgarn Craton consists predominantly of Archaean granite-greenstone rocks that were formerly subdivided into four provinces, namely the Western Gneiss Terrane (including the Narryer Gneiss Complex), the Murchison Province, the Southern Cross Province and the Eastern Goldfields Province (Gee et al., 1981). Myers (1993) suggested abandoning this subdivision in favour of four ‘superterranes’ and as many as twelve smaller tectono-stratigraphic terranes. Hence, the craton is now widely acknowledged to comprise an assemblage of several smaller terranes (e.g. Myers, 1993; Wilde et al., 1996) (Fig. 1). Further evidence for the amalgamation of smaller terranes is provided by seismic studies of the deep crustal structure of the southwestern Yilgarn Craton (Dentith et al., 2000).

SHRIMP U–Pb zircon geochronological data reported from the Yilgarn Craton revealed predominantly Archaean ages (Nelson, 1995, 1996, 1997a,b, 1998). Evidence for post-Archaean strata is recorded in Proterozoic basins, which developed primarily during the Glenburgh Orogeny (~2000 Ma) and the Capricorn Orogeny (~1800 Ma) when the Pilbara and Yilgarn Cratons were amalgamated and these unconformably overlie the Yilgarn Craton to the north

(Occhipinti et al., 1998, 2004; Pirajno and Occhipinti, 2000; Kinny et al., 2004). In addition, Upper Palaeoproterozoic or older age sediments overlie the southern margin of the Yilgarn Craton (e.g. Dawson et al., 2002). In the central Yilgarn Craton a quartz diorite has been dated at ~1215 ± 11 Ma (Qiu et al., 1999) and various dykes in the southern Yilgarn range between ~1204 and 1214 Ma (Wingate and Giddings, 2000; Pidgeon and Nemchin, 2001; Pidgeon and Cook, 2003). The timing of these intrusions suggests a possible link with events associated with the Mesoproterozoic Albany-Fraser Orogen located adjacent to the southern Yilgarn (Myers, 1990).

2.2. Phanerozoic

The collision of Gondwana and Laurasia forming the supercontinent Pangaea moved Australia into a near-polar position, leading to glacial conditions in Permo/Carboniferous time (Totterdell et al., 1990; Li and Powell, 2001). According to Totterdell et al. (1990) and Morgan (1993) the entire Western Australian Shield was probably covered by a continental ice sheet in the Late Carboniferous/Early Permian. Dickins (1996) proposed at least two cycles of glaciation during the Palaeozoic—one in the Namurian (Mid-Carboniferous) and another during the Asselian to Sakmarian (Early Permian). Evidence for glaciation is found in the form of Lower Permian tillites and glaciomarine sediments in the Perth Basin (Mory and Iasky, 1994) and in the Collie Basin (Le Blanc Smith, 1993). The Upper Carboniferous/Permian Paterson Formation comprises tillites and fluvioglacial sandstones and partly overlies the Proterozoic Rudall Metamorphic Complex (Chin et al., 1980). It also occurs as a stratigraphic unit in the Palaeozoic Gunbarrel Basin (Ghori, 1998), which onlaps the Yilgarn Craton to the east. This formation is correlated with the Upper Carboniferous/Lower Permian Grant Group of the Canning Basin to the northwest (Ghori, 1998). The finding of reworked Late Permian palynomorphs in Cretaceous sediments from the Great Australian Bight to the south of the Yilgarn Craton also suggests the presence of sediments of this age in the hinterland at the time of deposition, even though such sediments are no longer preserved (Alley and Clarke, 1992). The Permian sedimentary sequences in the Perth and Collie Basins are unconformably overlain by Cretaceous and Tertiary strata. The latter indicate palaeochannels and palaeodrainage areas of Early Eocene and younger age (Hocking and Cockbain, 1990; Morgan, 1993). Tertiary strata and the Yilgarn Craton itself are covered extensively by regolith varying in thickness from a few metres to over 150 m (Hocking and Cockbain, 1990; Anand and Paine, 2002).

Faults and mainly dolerite dykes cross-cut the Yilgarn Craton and their strike directions mainly reflect varying palaeo-stress regimes (e.g. Tyler, 1990; Dentith et al., 2000; Wingate and Giddings, 2000). Probably the most prominent structure is the Darling Fault (Fig. 1), a north–south trending fault along the western margin of the Yilgarn Craton separating it from the Phanerozoic Perth Basin. The basin acted as a depocentre for up to 15 km thickness of predominantly Permian to Jurassic clastic sediment (Harris, 1994; Song and Cawood, 2000).

3. Apatite fission track thermochronology

AFT thermochronology is an important tool with a wide range of applications, particularly in revealing the timing and magnitude of upper crustal tectonism and its consequences for surface processes (Gallagher et al., 1998; Gleadow et al., 2002b). Within the upper crust, temperature can often be used as a proxy for depth so that reconstructed cooling histories may be taken as a record of vertical rock movement towards the surface. For fluorapatites the temperature record is most sensitive in the range of ~110–60 °C (e.g. Gleadow et al., 1983; Laslett et al., 1987), which typically equates to crustal depths of ~2–5 km, depending on the geothermal gradient. Because of the temperature susceptibility of fission tracks in apatite to annealing, AFT data can be used to model thermal histories of samples. Using such modelled thermal histories and the assumption that cooling in the near-surface environment of the region investigated is dominated by tectonic and erosional denudation, permits the long-term denudation record of an area to be deduced. Only limited information is provided for temperatures below ~60 °C due in large part to the uncertainty of kinetic models of fission track behaviour. The basic principles and applications of the method are described in detail elsewhere

(Wagner and Van den Haute, 1992; Gallagher et al., 1998; Dumitru, 2000; Gleadow et al., 2002b).

4. Apatite fission track results

Sample preparation and methodology used in this study is explained in Appendix A. Sample information and analytical data are shown in Table 1. For convenience, samples are divided into four different groups according to location areas: west of the Darling Fault, Narryer Terrane, Murchison Terrane and Eastern Yilgarn Craton (Table 1).

Apparent AFT ages from the northern Yilgarn Craton range from 202 to 292 Ma with most falling between 202 and 250 Ma. To the west of the Darling Fault distinctly younger AFT ages of 146 ± 7 Ma and 150 ± 13 Ma are found in Precambrian crystalline basement, encountered at relatively shallow levels of 191 m and 248 m (Kohn et al., 2001) within the Woodleigh 1 well of the Woodleigh impact structure in the southern Carnarvon Basin (Fig. 1) (Reimold and Koeberl, 2000; Mory et al., 2001; Renne et al., 2002). These two samples have most likely experienced a different thermal history from samples on the Yilgarn Craton and are described in more detail by Kohn et al. (2001). Apart from the two Woodleigh samples the range of AFT ages is fairly restricted throughout the study area.

Mean track lengths of horizontally confined tracks (for which more than 35 tracks were measured) vary between 11.50 and 13.61 μm and are evenly distributed across the study area. Standard deviations of track length distributions range between 1.0 and 2.4 μm with few exceptions where only a few track lengths were available for measurement.

The mean of the horizontally confined track lengths versus the apparent AFT age of a sample is plotted in a so-called boomerang plot (Fig. 2). Boomerang plots are used to analyse regional FT data sets, i.e. a boomerang-shape of the data points may reveal times of accelerated cooling of a study area (Green et al., 1986; Gallagher et al., 1998). The boomerang plot in this study does not show a complete boomerang shape pattern of the data points or significant differences in the data with respect to location of the samples in the different areas.

Track length distribution histograms and radial plots of single grain age distributions for representative samples are shown in Fig. 3. The samples in Fig. 3 are selected to represent different areas, different apparent AFT ages, variations in MTL distributions as well as samples with low chi-square test results and samples where chlorine measurements are available. The track length distribution histograms are typically unimodal and usually contain a few short tracks. The radial plots of single grain ages show broad scatter of individual ages from a single population. No radial plots in this study show multiple populations of single grain ages.

4.1. Apatite chlorine content

In apatite, the degree of fission track annealing varies with duration of heating, chemical composition (Green et al., 1985; Barbarand et al., 2003) and mineralogical properties (Carlson et al., 1999). Although chlorine substitution probably exerts the most important effect on annealing, the possible influence of other trace elements (especially rare earths in chlorine-poor apatites) has also been reported by Barbarand et al. (2003). Chlorine-rich apatites for example, are more resistant to track annealing than fluorine-rich apatites and in the former total annealing of tracks may occur at higher temperatures between ~125 and 150 °C (e.g. Green et al., 1985; Burtner et al., 1994; O'Sullivan et al., 1995). One of the AFT age standards is Durango apatite, which has an average chlorine content of 0.41 wt.% and is classified as a fluorapatite (Barbarand et al., 2003). Since AFT data are commonly used for thermal history modelling the chlorine contents ideally of all evaluated grains should be measured—in practice usually a selection of representative samples is analysed.

Here five samples were selected for electron microprobe analysis. The samples were selected from different areas, representing different apparent AFT ages and different chi-square values. Electron microprobe analysis of 20 individual grains per sample, analysed previously for AFT age and length data, were carried out to estimate the chlorine content for five selected samples (Table 1). The authors acknowledge that the chlorine contents of the five analysed samples–all with average chlorine content below the Durango standard 0.41 wt.% chlorine–is no proof that

Table 1
Apatite fission track data from the northern Yilgarn Craton

Sample number	Long. E′	Lat. S′	Lithology	Elev. (m)	No. of grains	Standard track density $\times 10^6$ cm^{-2} (Nd)	Spontaneous track density $\times 10^6$ cm^{-2} (Ns)	Induced track density $\times 10^6$ cm^{-2} (Ni)	U (ppm)	χ^2 %	Fission track age $\pm 1\sigma$ (Ma)	Mean track length $\pm 1\sigma$ (μm)	SD (μm)	Range of Weight % chlorine[a]
West of Darling Fault														
88-30	115°11′10″	28°11′05″	gneiss	150	20	1.329 (5609)	1.535 (1594)	1.585 (1646)	15	37	233 ± 10	13.07 ± 0.18 (100)	1.79	0.00–0.01
89-457	115°11′10″	28°11′05″	granite	150	20	1.307 (5098)	0.828 (901)	0.725 (789)	7	98	270 ± 15	13.18 ± 0.16 (95)	1.57	0.00–0.01
FT26	114°38′42″	28°23′38″	granite	160	20	1.372 (4673)	2.118 (1334)	2.431 (1531)	22	88	217 ± 10	12.84 ± 0.15 (102)	1.50	–
Narryer Terrane														
105001	115°53′58″	26°58′11″	monzogran.	300	23	1.281 (5182)	3.072 (2016)	2.996 (1915)	29	78	238 ± 10	12.80 ± 0.16 (102)	1.64	–
105002	116°06′32″	26°47′36″	orthogneiss	330	22	1.300 (5182)	2.909 (2059)	2.706 (1966)	26	59	253 ± 10	12.51 ± 0.20 (101)	2.06	–
105004	116°01′26″	26°54′17″	monzogran.	290	21	1.319 (5182)	1.532 (1414)	1.496 (1381)	14	93	245 ± 11	12.33 ± 0.20 (100)	2.02	–
105005	115°53′40″	26°45′30″	orthogneiss	300	4	1.337 (5182)	4.179 (222)	4.010 (213)	38	13	252 ± 25	14.32 ± 0.31 (14)	1.14	–
105010	116°32′40″	26°14′00″	orthogneiss	340	20	1.356 (5182)	1.176 (658)	1.190 (666)	11	97	243 ± 15	12.58 ± 0.19 (100)	1.91	–
142896	117°14′37″	25°36′00″	gneiss	450	20	1.263 (5182)	4.949 (2823)	4.572 (2608)	45	2	255 ± 10	12.99 ± 0.18 (100)	1.75	0.08–0.52
142900	117°17′48″	25°20′30″	monzogran.	445	22	1.073 (4673)	0.771 (889)	0.724 (834)	8	99	208 ± 11	12.49 ± 0.16 (100)	1.63	–
142901	117°20′56″	25°34′41″	monzogran.	450	20	1.098 (4673)	2.387 (1920)	2.145 (1726)	24	70	222 ± 9	12.24 ± 0.15 (100)	1.52	–
142902	117°20′55″	25°34′40″	monzogran.	450	21	1.123 (4673)	1.192 (1667)	1.050 (1468)	12	97	231 ± 10	12.73 ± 0.13 (100)	1.26	–
142911	116°36′07″	25°36′48″	monzogran.	380	22	1.380 (4234)	1.993 (2602)	1.915 (2500)	17	5	260 ± 10	12.62 ± 0.16 (100)	1.64	–
142913	117°05′51″	25°38′14″	monzogran.	460	19	1.403 (4234)	5.274 (2393)	5.624 (2552)	50	35	238 ± 9	12.40 ± 0.17 (100)	1.74	–
159724	116°10′43″	25°07′35″	monzogran.	310	19	1.426 (4234)	1.376 (361)	1.391 (365)	12	100	255 ± 20	12.06 ± 0.16 (100)	1.89	–
159995	116°08′34″	25°05′10″	granodiorite	300	22	1.449 (4234)	0.513 (236)	0.578 (266)	5	100	233 ± 22	12.15 ± 0.23 (95)	2.27	–
84-96	116°07′30″	26°26′00″	granite	300	20	1.229 (5098)	1.474 (1547)	1.525 (1601)	16	99	216 ± 10	13.59 ± 0.12 (100)	1.17	–
87-305	117°21′10″	25°34′05″	granite	480	20	1.255 (5098)	3.535 (1964)	3.737 (2076)	37	88	215 ± 9	12.61 ± 0.15 (100)	1.55	–
88-187	115°57′55″	26°50′40″	paragneiss	310	20	1.410 (5609)	5.050 (2366)	4.677 (2191)	42	44	275 ± 11	13.61 ± 0.10 (100)	0.99	0.19–0.32
88-197	116°07′30″	26°32′30″	gneiss	335	20	1.573 (5609)	2.634 (2153)	2.938 (2401)	23	19	255 ± 10	13.12 ± 0.12 (100)	1.21	–
89-456	116°07′30″	26°26′00″	gneiss	300	20	1.281 (5098)	2.753 (2846)	2.677 (2767)	26	73	239 ± 9	13.01 ± 0.13 (104)	1.36	–
90-417	115°46′30″	28°50′00″	gneiss	300	20	1.152 (5098)	1.242 (1269)	1.248 (1275)	14	60	208 ± 10	12.04 ± 0.24 (101)	2.39	–
91-256	115°38′06″	25°35′50″	granite	300	20	1.204 (5098)	2.349 (1565)	2.202 (1467)	23	95	233 ± 10	12.33 ± 0.16 (101)	1.52	–
Murchison Terrane														
105011	116°54′15″	26°10′35″	granite	390	20	1.375 (5182)	1.017 (834)	0.980 (804)	9	99	258 ± 14	13.15 ± 0.18 (100)	1.84	–
105015	116°49′30″	26°29′40″	granite	440	20	1.393 (5182)	3.148 (2346)	3.065 (2284)	28	92	259 ± 10	12.50 ± 0.15 (105)	1.55	–
118963	119°15′30″	25°53′35″	syenogran.	600	20	1.449 (5182)	1.362 (525)	1.424 (549)	12	96	251 ± 17	12.34 ± 0.18 (100)	1.78	–

88-165	115°41′45″	27°24′55″	gneiss	275	20	1.383 (5609)	0.965 (918)	0.939 (893)	9	99	257 ± 14	12.99 ± 0.16 (101)	1.57	–
88-188	116°56′20″	26°12′00″	granite	390	20	1.438 (5609)	2.439 (2312)	2.539 (2407)	22	15	250 ± 10	13.03 ± 0.11 (103)	1.15	–
88-189	116°20′55″	27°06′35″	granite	350	20	1.465 (5609)	2.094 (1928)	2.418 (2226)	21	42	230 ± 9	12.72 ± 0.14 (102)	1.43	–
88-191	116°56′21″	26°12′03″	gneiss	390	20	1.492 (5609)	4.320 (3907)	4.824 (4362)	40	39	242 ± 8	12.88 ± 0.14 (100)	1.42	–
88-192	116°59′20″	26°14′40″	monzonite	370	20	1.519 (5609)	3.580 (2424)	4.013 (2717)	33	98	245 ± 9	12.96 ± 0.13 (100)	1.31	–
88-195	116°52′20″	26°30′48″	granite	330	20	1.546 (5609)	1.324 (1508)	1.463 (1667)	12	84	253 ± 11	12.86 ± 0.13 (100)	1.23	–
88-22	116°58′30″	26°17′30″	gneiss	350	20	1.275 (5609)	2.384 (3907)	2.024 (4362)	20	99	271 ± 12	13.02 ± 0.14 (102)	1.37	–
88-25	117°02′20″	26°07′00″	gneiss	380	21	1.302 (5609)	1.909 (3907)	1.868 (4362)	18	6	241 ± 10	13.38 ± 0.14 (100)	1.36	–
88-31	116°54′10″	26°11′05″	gneiss	390	14	1.356 (5609)	1.411 (448)	1.452 (461)	13	97	239 ± 17	12.78 ± 0.24 (42)	1.58	–
FT18	118°28′45″	26°34′55″	gneiss	510	18	1.248 (4673)	1.265 (523)	1.233 (510)	12	92	232 ± 16	12.43 ± 0.20 (100)	1.99	–
UW 98/1	116°48′37″	28°07′42″	diorite	110	17	1.188 (4285)	0.933 (592)	0.888 (563)	9	80	227 ± 15	11.50 ± 0.18 (81)	1.61	–
UW 98/2	116°59′54″	27°46′57″	granite	160	10	1.210 (4285)	3.539 (462)	3.316 (433)	34	91	234 ± 17	12.32 ± 0.20 (68)	1.69	
UW 98/3	117°27′39″	27°24′16″	granodiorite	140	8	1.234 (4285)	1.682 (702)	1.872 (781)	19	96	202 ± 12	12.80 ± 0.17 (75)	1.50	–
UW 98/4	117°43′24″	27°07′49″	granodiorite	125	20	1.258 (4285)	2.139 (2430)	1.997 (2269)	20	92	244 ± 10	12.83 ± 0.12 (99)	1.23	–
UW 98/44	119°01′30″	25°52′47″	arcose	560	9	1.290 (3788)	2.480 (273)	2.734 (301)	27	77	212 ± 19	12.99 ± 0.16 (79)	1.45	–
UW 98/46	118°35′24″	26°25′27″	granodiorite	550	20	1.309 (3788)	2.671 (1516)	2.704 (1535)	26	63	234 ± 11	12.23 ± 0.18 (106)	1.80	–
Eastern Yilgarn														
118936	120°26′00″	27°34′20″	granite	540	20	1.412 (5182)	1.614 (1244)	1.640 (1264)	15	54	251 ± 12	12.43 ± 0.21 (100)	2.09	–
118937	120°26′30″	27°34′40″	conglomer.	530	20	1.431 (5182)	2.660 (1466)	2.410 (1328)	21	100	285 ± 13	13.01 ± 0.13 (105)	1.38	–
142810	121°13′13″	27°27′50″	syenite	520	23	1.207 (5182)	3.032 (2115)	2.447 (1707)	25	90	270 ± 11	12.36 ± 0.18 (102)	1.81	0.00–0.01
142815	121°30′45″	26°34′00″	monzogran.	500	4	1.225 (5182)	0.349 (65)	0.284 (53)	3	98	271 ± 51	13.11 ± 0.30 (14)	1.10	–
142815	121°30′45″	26°34′00″	monzogran.	500	6	1.244 (5182)	0.409 (121)	0.315 (93)	3	97	292 ± 41	11.45 ± 0.78 (15)	3.01	–
FT 9	122°04′16″	28°45′00″	dacite	450	5	1.148 (4673)	0.391 (12)	0.423 (13)	5	87	193 ± 77	8.81 ± 4.09 (2)	5.78	–
FT10	122°04′00″	28°46′00″	syenite	450	11	1.173 (4673)	1.978 (247)	1.658 (207)	18	98	253 ± 25	11.76 ± 0.38 (35)	2.26	–
FT12	120°53′53″	28°28′00″	lamprophy.	400	9	1.198 (4673)	0.387 (29)	3.472 (26)	4	97	242 ± 66	13.03 ± 0.39 (38)	2.41	–
FT15	120°30′15″	27°19′40″	granite	550	20	1.222 (4673)	1.125 (845)	1.011 (760)	10	60	246 ± 14	12.40 ± 0.17 (101)	1.70	–

Ages determined by UDW using zeta = 369 ± 8 for dosimeter glass CN-5. Brackets show number of tracks counted. Standard and induced track densities measured on mica external detectors (g = 0.5), and fossil tracks densities on apatite surfaces. AFT ages are pooled ages for passed χ^2 test (>5%). If χ^2 test fails (<5%), then central age is used.

[a] Chlorine was determined on a JEOL JXA-5A electron microprobe running at an accelerating voltage of 15 kV, defocused beam size of 15–20 μm and beam current of 29 nA; samples were calibrated using the Durango apatite standard. For values <0.02% CI errors are about ± 100%, for values of ~0.10% CI errors are about ± 25%, and for values ~1% CI are about ± 15%. Analyses were performed at Geotrack International Pty Ltd.

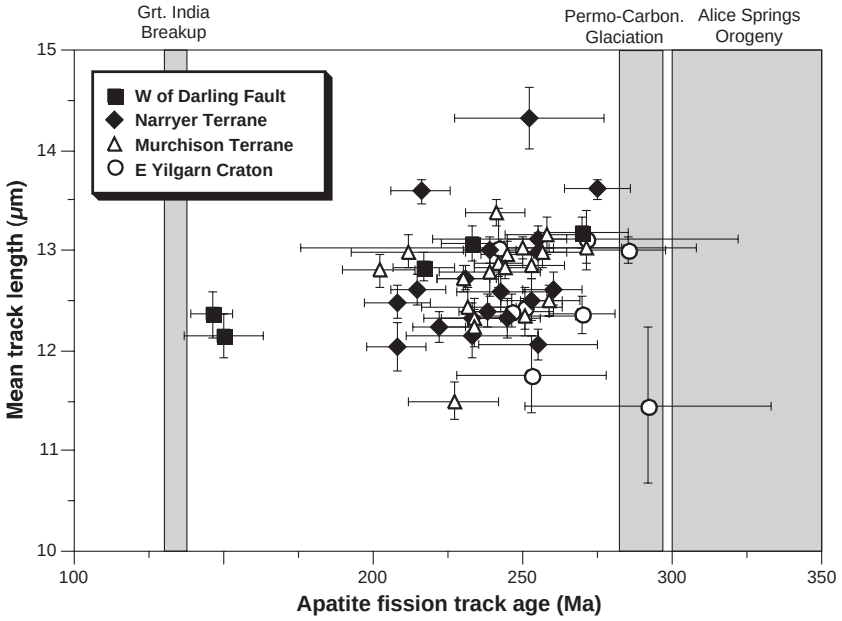

Fig. 2. Plot of mean track length versus AFT age with respect to local sample distribution (error bar is uncertainty at $\pm 1\sigma$). Different symbols are used for samples from the four key areas, as outlined in Table 1. Grey zones show the time range of various geological regional events. The figure shows the reasonably uniform AFT parameters (age and mean track length) of the samples throughout most of the study area.

the rest of the samples are also fluorine-rich samples. However, these results, as well as results from elsewhere on the craton (Kohn et al., 2002) and the statistical fact that most upper crustal apatites are fluorine-rich (Barbarand et al., 2003) strengthens our assumption that all samples in this study are fluorine-rich.

5. Data interpretation

The AFT age and length data is restricted in range over the study area (Fig. 3), therefore sample details shown in this figure are considered representative for the entire data set.

Evidence for a degree of track annealing is shown by the fact that all apparent AFT ages (Phanerozoic) are substantially younger than their Precambrian emplacement or metamorphic age and that mean track lengths (for which more than 35 tracks were measured) fall in the range of 11.50–13.61 μm. The track length histograms show a unimodal distribution of confined track lengths, suggesting slow and continuous cooling from temperatures >10 °C. This interpretation is also consistent with the boomerang plot (Fig. 2).

Interpretation of all these data indicates that the study area has experienced a single slow cooling event. According to the values of the apparent ages samples probably passed through ~110 °C sometime in the Late Carboniferous or Early Permian and then samples continued to cool below ~60 °C, most likely between Late Permian and Jurassic time. Below ~60 °C annealing of fission tracks in apatite is quite sluggish, but samples are presumed to have continued to cool reaching close to present-day surface temperatures in Jurassic–Cretaceous time.

The existence of few shorter horizontally confined track lengths may indicate an earlier heating event preceding the major cooling phase of the Late Carboniferous/Early Permian. In this case palaeotemperatures attained were sufficiently high to anneal most, but not all of the previously existing tracks.

To test this proposed general thermal history some modelling programs exist based on extrapolated results from laboratory annealing experiments. We have used such a computer model to test our thermal

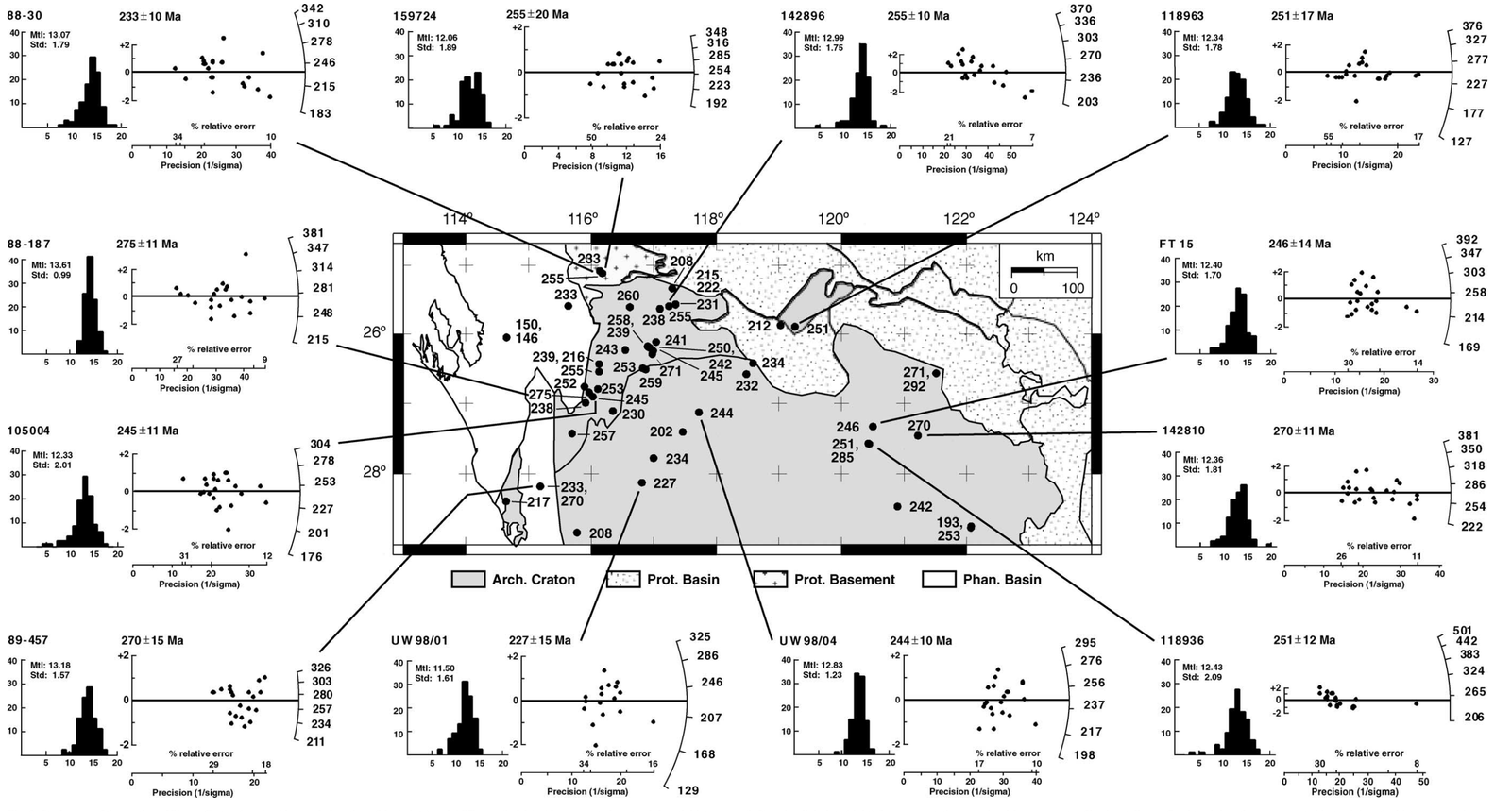

Fig. 3. Study area of the northern Yilgarn Craton (grey) with sample locations (black dots) and AFT ages (in Ma). Also presented are track length histograms (left) and radial plots (right) for representative samples. Measurements of horizontally confined track lengths are presented in track lengths histograms at 1 μm intervals. An apparent AFT age is based on a number of single grain ages which can be visualized in radial plots (Galbraith, 1988; Galbraith and Green, 1990). In radial plots, the slope of a straight line from the origin (0) is equivalent to the fission track age read off radially around the perimeter of the plot. The x value and the % relative error are a measure of the precision of each grain age. The further a point plots to the right of the origin, the more precise the individual grain age. If all grains belong to a single age population then they should scatter within the $\pm 2\sigma$ age range about the central age, outlined by the heavy line along the y-axis. Scatter outside this range indicates a spread of grain ages, which should also be reflected by the chi-square statistic. Age distributions in radial plots that pass the chi-square test at the 95% confidence level represent a single population of individual ages (Galbraith, 1981) (see also Table 1).

history interpretation. The procedure and results are explained in the following section.

6. Thermal history modelling

6.1. Background

Numerous time–temperature (*t–T*) scenarios are possible for AFT age results obtained from any given sample. However, when combined with fission track length details, the data allow more rigorous constraints to be placed on the interpretation of an observed age (Gleadow and Duddy, 1981). AFT age and length data reflect the time over which tracks have been retained in apatite and the thermal history of the host material. Integration of these two parameters can often differentiate uniquely between different thermal history types for temperatures below ~125–110 °C. This understanding is based on an empirical kinetic description of laboratory annealing data in Durango apatite (Green et al., 1986; Laslett et al., 1987).

Modelling of time–temperature (*t–T*) paths here follows the procedure outlined by Gallagher (1995). This procedure incorporates a forward modelling approach using a genetic algorithm, which uses a stochastic search method for simulating numerous possible *t–T* paths with statistical testing of the outcomes against the observed AFT ages and track length distributions. These are then refined using the 'Approximate Likelihood Ratio' test (Gallagher, 1995), which calculates the best data fitting thermal model and its 95% confidence region. Due the relative insensitivity of apatite annealing kinetics at temperatures <60 °C, thermal histories below this temperature should be considered poorly constrained.

For time–temperature modelling in this study, we chose all samples for which >50 measured horizontally confined track lengths were available and whose Cl content range was less than or close to that for Durango apatite (~0.41 wt.% Cl) (see Section 4.1). Altogether forty-three samples were used for time–temperature modelling of which three representative models are shown in Fig. 4. Samples were modelled using initial mean track lengths of 16.3 μm and 14.5 μm. Both values showed different thermal history scenarios, as suggested by Gunnell et al. (2003). However, for reasons described and explained by Kohn et al. (2001) and Gunnell et al. (2003) in this study only models with an initial track length value of 14.5 μm were adopted. In performing the modelling procedure, a wide range of *t–T* constraints are used covering the interval from Mid-Palaeozoic to present. It is possible to model a range of different thermal histories for a particular sample, which all concur with the data. However, not all of these histories are consistent with the geological constraints. Here, the AFT data are modelled in two ways, using different geological constraints as outlined below in more detail.

6.2. Thermal history models for the Northern Yilgarn Craton

Models presented in Fig. 4 are calculated using an initial mean track length of 14.5 μm (Kohn et al., 2001; Gunnell et al., 2003). The three models shown in Fig. 4a predict a single stage cooling history that is consistent with the stratigraphic record in adjacent sedimentary basins. These fairly unconstrained thermal history models indicate cooling from >110 °C starting in the Late Carboniferous/Early Permian and cooling continuing to temperatures <60 °C by Early- to Mid-Jurassic time (Fig. 4a). The subsequent thermal history path between <60° and ~20 °C is less well constrained due to a lack of sensitivity of the AFT thermochronometer over this temperature range.

In a second set of models (Fig. 4b) two additional geological constraints are added to the thermal history modelling: Firstly, Lower Permian periglacial sedimentary remnants unconformably overlying the western and eastern margin of the Yilgarn Craton imply that at least parts of the present craton surface were exposed during the Permo/Carboniferous Gondwana glaciation. However, it is unlikely that the present day surface has remained exposed since the Late Palaeozoic. Also AFT data presented here suggest cooling of the present day outcropping rocks at sometime in the Permian. One possible explanation for this apparent paradox may be that a sedimentary blanket covered the shield sometime post-Early Permian.

Secondly, vitrinite reflectance data from Permian coal measures from the Collie Basin (Fig. 1) in the

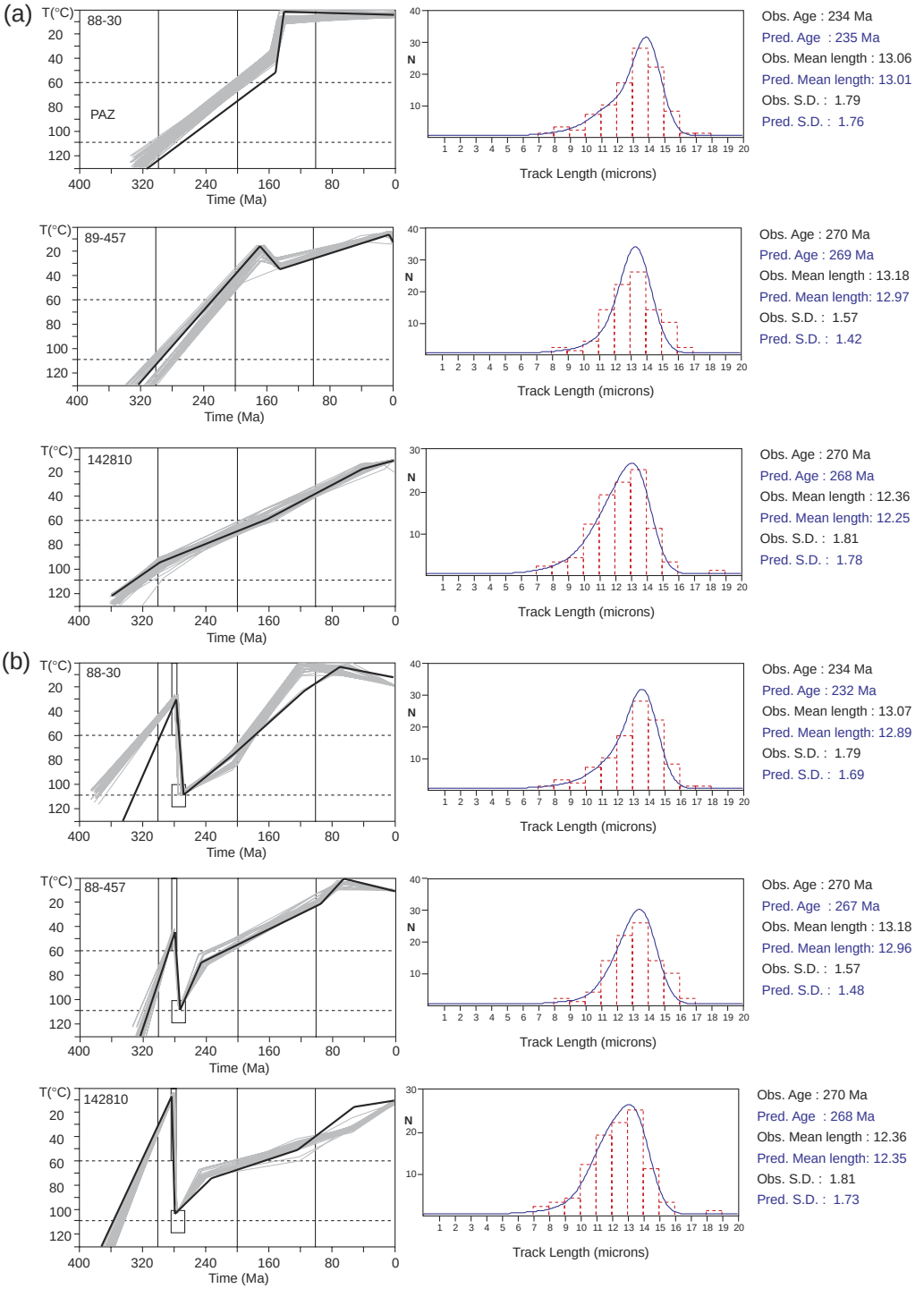
(a)
T(°C)
88-30
PAZ
Time (Ma)
N
Track Length (microns)
Obs. Age : 234 Ma
Pred. Age : 235 Ma
Obs. Mean length : 13.06
Pred. Mean length: 13.01
Obs. S.D. : 1.79
Pred. S.D. : 1.76
89-457
Obs. Age : 270 Ma
Pred. Age : 269 Ma
Obs. Mean length : 13.18
Pred. Mean length: 12.97
Obs. S.D. : 1.57
Pred. S.D. : 1.42
142810
Obs. Age : 270 Ma
Pred. Age : 268 Ma
Obs. Mean length : 12.36
Pred. Mean length: 12.25
Obs. S.D. : 1.81
Pred. S.D. : 1.78
(b)
88-30
Obs. Age : 234 Ma
Pred. Age : 232 Ma
Obs. Mean length : 13.07
Pred. Mean length: 12.89
Obs. S.D. : 1.79
Pred. S.D. : 1.69
88-457
Obs. Age : 270 Ma
Pred. Age : 267 Ma
Obs. Mean length : 13.18
Pred. Mean length: 12.96
Obs. S.D. : 1.57
Pred. S.D. : 1.48
142810
Obs. Age : 270 Ma
Pred. Age : 268 Ma
Obs. Mean length : 12.36
Pred. Mean length: 12.35
Obs. S.D. : 1.81
Pred. S.D. : 1.73

southwestern Yilgarn Craton imply a maximum burial temperature of ~100 °C (Le Blanc Smith, 1993). This observation suggests the presence of an additional Phanerozoic cover to the ~1.4 km presently preserved in the Collie Basin. However, the Collie coal is developed and preserved within a graben, so its thermal history might not be representative for the entire craton.

Considering these two variables as being applicable to the study area, the time–temperature constraints for the thermal history modelling of the samples are refined and tested in the second set of models (Fig. 4b).

In this second modelling series the samples are constrained to have been exposed to estimated surface temperatures in the Early Permian followed by rapid burial to reach temperatures ~100 °C by late Early Permian time. All samples modelled using these geological constraints indicate rapid burial in the Early Permian reaching temperatures >100 °C followed by continuous slow cooling. The AFT data predicted by the thermal models also closely match the observed age and mean track length data.

6.3. Thermal history models of adjacent basins

Additional AFT data from boreholes in the Carnarvon Basin have been reported (e.g. Gibson et al., 1998, 2000; Hegarty et al., 1998; Ghori, 1999; Crostella et al., 2000). These apatites originate from sedimentary rocks and four different cooling events in the Phanerozoic are identified in the reconstructed thermal histories, i.e. in the Permian, Middle/Late Jurassic, Early Cretaceous and Late Tertiary. The data suggest that the surrounding Phanerozoic sedimentary basins experienced different and later thermal histories compared to the thermal history of the northern Yilgarn Craton.

7. Discussion

As evident from Fig. 4 both modelling approaches are equally likely and yield good fits between predicted and observed data. Both thermal history styles indicate relatively slow cooling histories from Permian through to Mesozoic times. The only differences between both modelling approaches are the two additional geological constraints added to the modelling in Fig. 4b. These models are in good agreement with the assumption that rapid burial occurred in the Early Permian—as indicated by vitrinite reflectance data from the Collie Basin, south of the study area. Here the models suggest rapid burial of the northern part of the Yilgarn Craton in the Early Permian followed by slow monotonic cooling through to Early to Mid-Jurassic time (Fig. 4b).

AFT thermal history information may be related to thermal relaxation following increased heat-flow (for example related to rifting), to localised magmatism, hot fluid flow or to denudation at the land surface. For the study area, elevated heat flow and magmatism as the primary cause of annealing over a relatively large continental area is largely ruled out. Further, the movement of hydrothermal fluids in former cover successions or crystalline basement may influence the AFT pattern in some cases but generally this is viewed as a more localised effect and the relative homogeneity of the AFT data in the study area would also tend to exclude this possibility. Hence, we consider that most cooling in the near-surface environment of the northern Yilgarn Craton is dominated by erosional denudation.

7.1. How much denudation has occurred?

Sparse heat flow measurements for the Western Australian Shield range between 40–50 mW m^{-2} (Cull, 1982; Morgan, 2000). Assuming an average

Fig. 4. Time–temperature plots for three selected samples (see Table 1) from the study region representing a common thermal history, which is observed in most samples. Models are derived using the AFT data and the genetic algorithm forward modelling procedures described by Gallagher (1995). Model paths shown (left panel) all predict resulting fission track parameters, which closely match the observed fission track parameters. In the right panel the predicted fission track parameters for the best individual run for a particular sample are compared to those measured. These are also shown as track length histograms (measured data) compared with a curve predicted from the model. Thermal histories in (a) are totally unconstrained by geological input compared to those shown in (b) (see text for further discussion on modelling and geological constraints). Thermal histories in (b) are constrained to reconcile possible rapid burial in the Early Permian to temperatures >~100 °C, followed by slower cooling through to early Mid-Jurassic time, when samples cool to below the partial annealing zone (PAZ), i.e. <~60 °C. In this case, since the AFT models suggest substantial reheating upon burial, the pre-Early Permian history is poorly constrained.

thermal conductivity of 2.5 W m^{-1} $°C^{-1}$ (Veevers, 2000) for upper crustal rocks, a present day average geothermal gradient of ~18 ± 2 °C km^{-1} can be calculated. If this geothermal gradient was prevalent throughout Phanerozoic time then a minimum of ~50 °C of Early Permian to early Mid-Jurassic cooling (from ~110 to 60 °C) is predicted by the AFT modelling, which suggests denudation of ~2.5–3.1 km. Assuming that the palaeosurface elevation was maintained at present day levels, this thickness translates into an average denudation rate of ~30 m $m.y.^{-1}$ This denudation rate is substantially greater than the ~0.1–0.2 m $m.y.^{-1}$ based on geomorphological evidence for the West Australian Shield (Finkl and Fairbridge, 1979; Fairbridge and Finkl, 1980) and that of 0–2 m $m.y.^{-1}$ for the Yilgarn Craton (Gale, 1992).

However, the results reported here are supported by other studies indicating that burial and exhumation contributed to the subaerial preservation of ancient Australian landforms (e.g. Kohn et al., 2002; Belton et al., 2004).

7.2. What happened to the denuded material?

A number of indicators, discussed in the previous section, imply the burial of the present-day surface of the Western Australian Shield in Late Carboniferous to Early Permian time followed by denudation of ~2.5–3.1 km from the northern Yilgarn Craton. The surrounding Phanerozoic basins (Fig. 1) are potential depocentres for the denuded material. Adjacent basins to the northern Yilgarn Craton are the Perth Basin to the west, the Gunbarrel Basin to the east and the Eucla Basin to the south, although the last one contains very few Palaeozoic sediments.

The Perth Basin directly overlaps the shield onshore and continues offshore in a series of platforms, troughs and subbasins with complicated basin structures. The basin contains mainly clastic sediments of Permian (~3 km) and Triassic/Jurassic (>10 km) age (Song and Cawood, 2000). With the final separation of Greater India from the Australian continent (Song and Cawood, 2000) in the Neocomian sedimentation in the Perth Basin ceased.

The Gunbarrel Basin unconformably overlies the Officer Basin to the east of the craton. Oldest strata are Ordovician volcanics and these pass up into Devonian sandstones (Apak et al., 2002). The Paterson Formation mainly consists of Permian tillites and fluvioglacial to lacustrine sandstone and claystone. Triassic and Jurassic deposition are absent and may have been eroded before a thin layer of Lower Cretaceous clastics has been deposited, which now covers unconformably the Permian sequences.

These findings show that clastic sedimentation in the surrounding Phanerozoic basins coincides with the major denudation phase based on thermal models of AFT data from the northern Yilgarn Craton.

7.3. Sediment provenance in Phanerozoic basins

Considerable clastic sedimentation has occurred in the Phanerozoic Gunbarrel and Perth Basins in Late Palaeozoic to Mid-Mesozoic time. The plate tectonic setting of the Yilgarn Craton during this interval suggests a variety of possible sedimentary source regions, including Antarctica, Greater India and the Cimmerian Blocks (Metcalfe, 1996).

SHRIMP U–Pb dating of detrital zircons is used as a source indicator for sediment provenance studies (Morton et al., 1991). Detrital zircon studies from Quaternary sands along the south west coastline of Western Australia by Sircombe and Freeman (1999) show that they are dominated by Meso- and Neoproterozoic ages, rather than the Archaean ages that may be expected from erosion of the adjacent Archaean shield area. The Albany-Fraser Orogen and the Leeuwin Complex of the Pinjarra Orogen (Fig. 1) have been identified as possible source regions for the recycled Perth Basin sediments, accumulated recently along the southwest Australian coastline (Sircombe and Freeman, 1999).

SHRIMP U–Pb dating of detrital zircons from the Perth Basin by Cawood and Nemchin (2000) shows that zircons from the Ordovician Tumblagooda Sandstone, Lower and Upper Permian sequences and from the Lower Triassic are derived from multiple sediment sources. However, the Permo/Triassic sedimentary rocks are dominated by Meso- and Neoproterozoic zircons, with only a minor contribution from the Archaean Yilgarn Craton (Cawood and Nemchin, 2000). The results also imply a major provenance change in the Early Triassic, since the Kockatea Shale is dominated by Mesoproterozoic zircons with a marked absence of Archaean and post-Mesoproterozoic zircon ages (Cawood and Nemchin, 2000). This

suggests that the relief of the Yilgarn Craton during Late Palaeozoic–Early Mesozoic time was very subdued, or that the Yilgarn Craton was covered by Proterozoic or Palaeozoic sediments (Kohn et al., 2002). Cawood and Nemchin (2000) suggest that the Albany-Fraser Orogen and East Antarctic Craton are a major source, shedding Mesoproterozoic sediment from south to north, parallel to the basin axis of the Perth Basin. This view is also supported by others (Tewari and Veevers, 1993; Veevers, 2000; Veevers et al., 2005) who propose a radial drainage system from the East Antarctic Upland and the Mirny Highland (Fig. 5), which was active in the Permian shedding sediment onto the Australian continent at least as far as the Collie Basin.

Concluding on these findings it appears that most of the Perth Basin sediment was sourced from Proterozoic orogens primarily to the south and that the northern Archaean Yilgarn Craton may have been covered by several kilometers of post-Mesoproterozoic or Palaeozoic sediment, as also suggested by Kohn et al. (2002) and Veevers et al. (2005).

7.4. Tectonic setting and driving forces

To understand the fundamental causes of the cooling history of the northern Yilgarn Craton, it is necessary to consider the Mid-Palaeozoic to recent palaeogeographic and tectonic evolution of the study region.

At ~320 Ma Australia was part of Gondwanaland and Laurasia, which had collided to form the supercontinent Pangaea. In Australia this event is recorded by the culmination of the Alice Springs Orogeny,

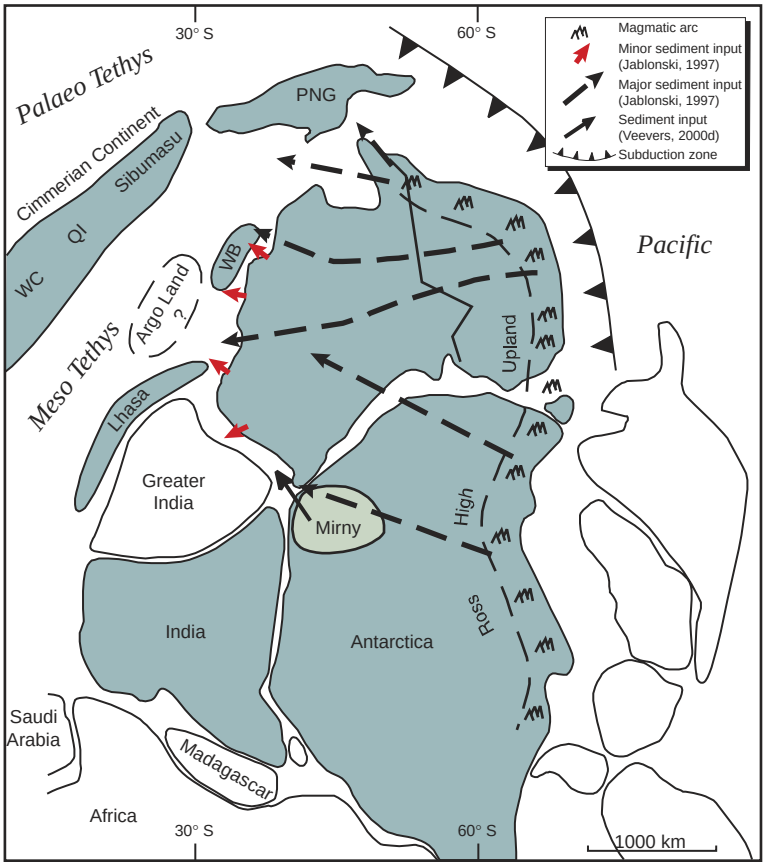

Fig. 5. Early Triassic palaeogeographic setting of Australia including proposed sediment transport directions (modified after Metcalfe, 1996; Jablonski, 1997; Veevers, 2000). PNG=Papua New Guinea, QI=Qiangtang, WB=West Burma, WC=Western Cimmeria.

which mostly affected central Australia but has also been detected in the Mt. Isa region (Haines et al., 2001; Spikings et al., 2001) and in the Mt. Painter region, Flinders Ranges (Mitchell et al., 1998, 2002; McLaren et al., 2002) (Fig. 1). At that time Gondwanaland, including Australia, had moved towards the South Pole, which triggered episodes of large scale glaciation commencing in the Late Carboniferous (Baillie et al., 1994; Dickins, 1996). By the Early Permian sea level had risen due to the melting ice sheet and sedimentation commenced in the surrounding basins. The dispersal of Pangaea (Fig. 5) commenced and the Cimmerian and Sibumasu Blocks separated from the North West Shelf around 270 Ma (Metcalfe, 1996). Sibumasu consisted of blocks now forming parts of Burma, Thailand, West Malaysia and northwest Sumatra (Metcalfe, 1988). In the Permo/Triassic, Pangaea commenced breaking up into different terranes accompanied by widespread volcanism. In the Canning Basin volcanism and dyke intrusion were also recorded around this time with AFT ages of 255 and 275 Ma (Gleadow and Duddy, 1984). At ~155 Ma West Burma and Argoland broke off the North West Shelf and drifted northwards (Gradstein and Ludden, 1992; Müller et al., 1998). However, the radiometric ages thought to record this event are inconsistent with biostratigraphic ages, which suggest a later breakup age of ~140 Ma (Gradstein and Ludden, 1992). The final separation of Greater India from Australia, marked by the record of sea floor spreading in the Indian Ocean, was established by 136 Ma (Müller et al., 1998). Around 85 Ma sea floor spreading progressed in the south, leading to the separation of Australia from Antarctica (Norvick and Smith, 2001).

At ~300 Ma the compressional regime (Alice Springs Orogeny) changed to an extensional one and Gondwanaland began to disperse. Subsidence created sag basins adjacent to the shield, which probably created sufficient geomorphological contrast to induce denudation on the Western Shield.

7.5. Discussion of AFT models

One possible interpretation of the AFT data presented here is that differential uplift of the western Yilgarn margin compared to the eastern part of the craton could have changed the palaeodrainage pattern, an idea also suggested by the Rb–Sr data of Libby et al. (1999). This would have led to the development of a drainage system dominated by flow to the east and may explain the apparent lack of Archaean sediment from the Yilgarn Craton to the Perth Basin. In this case, sediment in the Perth Basin could have originated from Greater India to the west, Antarctica or other adjacent crustal blocks. The sediment in the Gunbarrel Basin, however, is Permian in age and there is no great thickness of Triassic or Jurassic sediment, as predicted by our AFT thermal history models.

An alternative interpretation of the AFT data suggests burial of the northern Yilgarn Craton in the Early Permian followed by a prolonged period of denudation induced by the development of rifts along the western margin, in response to the onset of breakup of Gondwanaland. The sedimentary material possibly consisted of reworked Proterozoic and Lower Palaeozoic sediment, which may have been eroded into the developing Perth Basin to the west, causing the onset of cooling to be recorded in the underlying shield. This interpretation predicts a prolonged history of denudation, which can be readily reconciled with continuous clastic sedimentation into the adjacent Perth Basin.

8. Conclusions

Interpretation of the AFT data suggests the denudation of ~3 km of material from the northern Yigarn Craton during late Early Permian through to early Mid-Jurassic time at an average rate of ~30 m m.y.$^{-1}$ There is no evidence for an abnormal geothermal gradient prevailing at this time. Alternatively, the pattern of U–Pb ages of detrital zircons from the Perth Basin and vitrinite reflectance data from the Collie Basin in the southwest Yilgarn Craton suggest that the Australian Shield may have been buried under reworked Proterozoic and Palaeozoic sediment in Early Permian time. Both thermal history scenarios presented here are feasible and equally likely. The nature of the denudation, however, whether continuous or episodic, cannot be resolved by the present data. Denudation occurred either as a response to the waning stages of the Alice Springs Orogeny or was triggered by the breakup and dispersal of the supercontinent Pangaea, a relatively short time after its formation at ~300 Ma. Breakup may have led to the

development of contrast in geomorphic relief, which developed between the shield and the surrounding sag basins as a result of the extensional regime. This tectonic setting may have triggered the slow continuous denudation recorded from the northern Yilgarn Craton during Early Permian through to Mid/Late Jurassic time.

Acknowledgements

Funding for this work was provided by the Australian Geodynamic Cooperative Research Centre (AGCRC), the Australian Institute of Nuclear Science and Engineering (AINSE) and the Australian Research Council (ARC). UDW was supported by La Trobe and Melbourne Universities Postgraduate Scholarships. A. Nutman, P. Jackson, P.D. Fleming and A. Mory are thanked for providing sample material for this study. The authors would like to thank Paul O'Sullivan and Sandra McLaren for their thorough reviews, which greatly improved the manuscript.

Appendix A. Methodology

Sixty-three samples were assembled from the northern Yilgarn Craton of which fifty yielded sufficient apatite for fission track analysis. Samples were collected during field work and additional material was provided from mineral splits previously separated from samples prepared for SHRIMP U–Pb zircon analysis (Nutman et al., 1993; Nelson, 1995, 1996, 1997b, 1998, 1999). Apatite grains in the 63–250 μm size range were concentrated using standard magnetic and heavy liquid techniques. Apatite aliquots for analysis were mounted in epoxy resin on glass slides and ground and polished to an optical finish to expose internal grain surfaces. The mounts were etched in 5 M HNO_3 for 20 s at room temperature to reveal the fossil tracks. The external detector method was used for age determinations with Brazil Ruby muscovite attached to the sample to record induced tracks (Gleadow and Lovering, 1978; Hurford and Carter, 1991). The thermal neutron fluence was monitored by measuring the track density in muscovite plates attached to the Corning-5 standard glass (~12.5 ppm U). Neutron irradiations were carried out in the well-thermalised X-7 position of the Australian HIFAR Research Reactor at Lucas Heights, NSW, Australia. Following irradiation, muscovite detectors were etched for 27 min in 48% HF at room temperature to reveal induced tracks. Track counting and horizontal confined track length measurements were performed with a Zeiss Axiotron microscope under transmitted light, using a dry ×100 objective at a total magnification of ×1250.

Wherever possible, fission tracks in 20 suitable apatite grains per sample were counted and ages were calculated using the zeta calibration method and standard fission track age equation (Hurford and Green, 1982, 1983). Uncertainties were calculated using the techniques of Green (1981) and are expressed at the $\pm 1\sigma$ level (Table 1). The observed age spread was determined statistically using the chi-square test, which indicates the probability that all grains counted belong to a single population of ages (Galbraith, 1981). For samples which passed the chi-square test (i.e. a probability of $<5\%$) the 'central age' (Galbraith and Laslett, 1993) is concordant with the 'pooled age' within uncertainties. Ages in Table 1 were given as pooled ages, central ages were used only where samples did not pass the chi-square test.

Only fully etched and horizontal confined track lengths (HCTL) were measured in grains with polished surfaces parallel to the crystallographic *c*-axis (Laslett et al., 1982). Suitable HCTL were measured using a projection tube and a digitising tablet calibrated using a stage micrometer. For this procedure, the same magnification as for counting was applied, and the maximum possible number of suitable HCTL observed were measured in the entire mount prepared for any particular sample.

References

Alley, N.F., Clarke, J.D.A., 1992. Stratigraphy and palynology of Mesozoic sediments from the Great Australian Bight area, southern Australia. BMR Journal of Australian Geology and Geophysics 13, 113–130.

Anand, R.R., Paine, M., 2002. Regolith geology of the Yilgarn Craton, Western Australia: implications for exploration. Australian Journal of Earth Sciences 49, 3–162.

Apak, S.N., Ghori, K.A.R., Carlsen, G.M., Stevens, M.K., 2002. Basin development with implications for Petroleum Trap Styles

of the Neoproterozoic Officer Basin, Western Australia. In: Keep, M., Moss, S.J. (Eds.), The Sedimentary Basins of Western Australia: Proceedings of Petroleum Exploration Society of Australia Symposium, Perth, vol. 3, pp. 913–927.

Baillie, P.W., Powell, C.M., Li, Z.X., Ryall, A.M., 1994. The tectonic framework of Western Australia's Neoporoterozoic to recent sedimentary basins. In: Purcell, P.G., Purcell, R.R. (Eds.), The Sedimentary Basins of Western Australia: Proceedings of Petroleum Exploration Society of Australia Symposium, Perth, pp. 45–62.

Barbarand, J., Carter, A., Wood, I., Hurford, A.J., 2003. Compositional and structural control of fission-track annealing in apatite. Chemical Geology 198 (1–2), 107–137.

Belton, D.X., Brown, R.W., Kohn, B.P., Fink, D., Farley, K.A., 2004. Quantitative resolution of the debate over antiquity of central Australian landscapes and implications for the tectonic and geomorphic stability of cratonic interiors. Earth and Planetary Science Letters 219, 21–34.

Burtner, R.L., Nigrini, A., Donelick, R.A., 1994. Thermochronology of Lower Cretaceous source rocks in the Idaho-Wyoming Thrust Belt. American Association of Petroleum Geologists Bulletin 78 (10), 1613–1636.

Carlson, W.D., Donelick, R.A., Ketcham, R.A., 1999. Variability of apatite fission-track annealing kinetics: I. Experimental results. American Mineralogist 84, 1213–1223.

Cawood, P.A., Nemchin, A.A., 2000. Provenance record of a rift basin: U/Pb ages of detrital zircons from the Perth Basin, Western Australia. Sedimentary Geology 134, 209–234.

Chin, R.J., Williams, I.R., Williams, S.J., Crowe, R.W.A., 1980. Rudall – Western Australia, 1:250000 Geological Series – Explanatory Notes. Geological Survey of Western Australia, Perth, p. 22.

Crostella, A., Iasky, R.P., Blundell, K.A., Yasin, A.R., Ghori, K.A.R., 2000. Petroleum geology of the Peedamullah Shelf and Onslow Terrace, Northern Carnarvon Basin, Western Australia. Western Australia Geological Survey, Report, 73, Perth.

Cull, J.P., 1982. An appraisal of Australian heat-flow data. BMR Journal of Australian Geology and Geophysics 7, 11–21.

Daniels, J.L., 1975. Palaeogeographic development of Western Australia—Precambrian. Geological Survey of Western Australia Memoir 2, 437–450.

Dawson, G.C., Krapez, B., Fletcher, I.R., McNaughton, N.J., Rasmussen, B., 2002. Did late Palaeoproterozoic assembly of proto-Australia involve collision between the Pilbara, Yilgarn and Gawler Cratons? Geochronological evidence from the Mount Barren Group in the Albany-Fraser Orogen of Western Australia. Precambrian Research 118, 195–220.

Dentith, M.C., Dent, V.F., Drummond, B.J., 2000. Deep crustal structure in the southwestern Yilgarn Craton, Western Australia. Tectonophysics 325, 227–255.

Dickins, J.M., 1996. Problems of a Late Palaeozoic glaciation in Australia and subsequent climate in the Permian. Palaeogeography, Palaeoclimatology, Palaeoecology 125, 185–197.

Dumitru, T.A., 2000. Fission-track geochronology. In: Noller, J.S., Sowers, J.M., Lettis, W.R. (Eds.), Quaternary Geochronology: Methods and Applications. American Geophysical Union, Washington, DC, pp. 131–155.

Dunlap, W.P., Teyssier, C., 1995. Paleozoic deformation and isotopic disturbance in the southeastern Arunta Block, central Australia. Precambrian Research 71 (1–4), 229–250.

Fairbridge, R.W., Finkl, C.W., 1980. Cratonic erosional unconformities and peneplains. Journal of Geology 88, 69–86.

Finkl, C.W., Fairbridge, R.W., 1979. Paleogeographic evolution of a rifted cratonic margin: S.W. Australia. Palaeogeography, Palaeoclimatology, Palaeoecology 26, 221–252.

Galbraith, R.F., 1981. On statistical models for fission track counts. Mathematical Geology 13, 438–471.

Galbraith, R.F., 1988. Graphical display of estimates having differing standard errors. Technometrics 30 (3), 271–281.

Galbraith, R.F., Green, P.F., 1990. Estimating the component ages in a finite mixture. Nuclear Tracks 17 (3), 197–206.

Galbraith, R.F., Laslett, G.M., 1993. Statistical models for mixed fission track ages. Nuclear Tracks 21 (4), 459–470.

Gale, S.J., 1992. Long-term landscape evolution in Australia. Earth Surface Processes and Landforms 17, 323–343.

Gallagher, K., 1995. Evolving temperature histories from apatite fission-track data. Earth and Planetary Science Letters 136, 421–435.

Gallagher, K., Brown, R.W., Johnson, C., 1998. Fission track analysis and its applications to geological problems. Annual Review Earth and Planetary Sciences 26, 519–572.

Gee, R.D., Baxter, J.L., Wilde, S.A., Williams, I.R., 1981. Crustal development in the Yilgarn Block. In: Groves, D.I. (Ed.), Archaean Geology, Western Australia Geological Society of Australia, Special Publication, Perth, pp. 43–56.

Ghori, K.A.R., 1998. Petroleum generating potential and thermal history of the Neoproterozoic Officer Basin, Western Australia. In: Purcell, P.G., Purcell, R.R. (Eds.), Proceedings of Petroleum Exploration Society of Australia Symposium, Perth, The Sedimentary Basins of Western Australia, vol. 2, pp. 717–730.

Ghori, K.A.R., 1999. Silurian–Devonian petroleum source-rock potential and thermal history, Carnarvon Basin, Western Australia. Western Australia Geological Survey, Report 72, Perth.

Gibson, H.J., Marshallsea, S.J., Watson, P.G.F., 1998. Thermal history reconstruction in Carnarvon Basin wells Barrabiddy 1A, Yaringa East 1, Coburn 1 and an outcrop sample using apatite fission-track analysis and vitrinite reflectance. A report prepared for the Petroleum Exploration Initiatives Group of the Geological Survey of Western Australia, Geotrack International Pty Ltd (GEOTRACK), Report 670: Western Australia Geological Survey, S-series, S31321 A1 (unpublished).

Gibson, H.J., O'Brien, C., Watson, P.G.F., 2000. Thermal history reconstruction in Carnarvon Basin wells Candace 1, Pendock 1, Wandagee 1, Woodleigh 2A and Echo Bluff 1 using apatite fission track analysis and vitrinite reflectance. A report prepared for the Department of Minerals and Energy, Western Australia, Geotrack International Pty Ltd (GEOTRACK), Report 764, S-series, S31450 A1 (unpublished).

Gleadow, A.J.W., Duddy, I.R., 1981. A natural long-term track annealing experiment for apatite. Nuclear Tracks 5 (1/2), 169–174.

Gleadow, A.J.W., Duddy, I.R., 1984. Fission track dating and thermal history ananlysis of apatites from wells in the north-

west Canning Basin. In: Purcell, P.G. (Ed.), The Canning Basin, Western Australia Proceedings of the Geological Society of Australia/Petroleum Exploration Society of Australia Symposium, Perth, pp. 377–387.

Gleadow, A.J.W., Lovering, J.F., 1978. Thermal history of granitic rocks from western Victoria: a fission track dating study. Journal of Geological Society Australia 25, 323–340.

Gleadow, A.J.W., Duddy, I.R., Lovering, J.F., 1983. Apatite fission track analysis as a palaeotemperature indicator for hydrocarbon exploration. Australian Petroleum and Exploration Association Journal 23, 93–102.

Gleadow, A.J.W., Kohn, B.P., Brown, R.W., O'Sullivan, P.B., Raza, A., 2002a. Fission track thermotectonic imaging of the Australian continent. Tectonophysics 349, 5–21.

Gleadow, A.J.W., Belton, D.X., Kohn, B.P., Brown, R.W., 2002b. Fission track dating of phosphate minerals and the thermochronology of apatite. In: Hughes, J.M., Kohn, M.J., Rakovan, J. (Eds.), Phosphates: Geochemical, Geobiological and Materials Importance. Reviews in Mineralogy and Geochemistry, pp. 579–630.

Gradstein, F.M., Ludden, J.N., 1992. Radiometric age determinations for basement from sites 765 and 766, Argo abyssal plain and northwestern Australian margin. Proceedings of the Ocean Drilling Program, Scientific Results 123, 557–559.

Green, P.F., 1981. A new look at statistics in fission-track dating. Nuclear Tracks 5 (1/2), 77–86.

Green, P.F., Duddy, I.R., Gleadow, A.J.W., Tingate, P.R., Laslett, G.M., 1985. Fission track annealing in apatite: track length measurements and the form of the Arrhenius plot. Nuclear Tracks 10, 323–328.

Green, P.F., Duddy, I.R., Gleadow, A.J.W., Tingate, P.R., Laslett, G.M., 1986. Thermal annealing of fission tracks in apatite: 1. A qualitative description. Chemical Geology 59, 237–253.

Gunnell, Y., Gallagher, K., Carter, A., Widdowson, M., Hurford, A.J., 2003. Denudation history of the continental margin of western peninsular India since the early Mesozoic—reconciling apatite fission-track data with geomorphology. Earth and Planetary Science Letters 6761, 1–15.

Haines, P.W., Hand, M., Sandiford, M., 2001. Palaeozoic synorogenic sedimentation in central and northern Australia: a review of distribution and timing with implications for the evolution of intracontinental orogens. Australian Journal of Earth Sciences 48, 911–928.

Harris, L.B., 1994. Structural and tectonic synthesis for the Perth Basin, Western Australia. Journal of Petroleum Geology 17 (2), 129–156.

Hegarty, K.A., Moore, M.E., Watson, P.G.F., 1998. Quail 1 well, Carnarvon Basin, thermal history reconstruction using apatite fission-track analysis and vitrinite reflectance. A report prepared for the Geological Survey of Western Australia, Geotrack International Pty Ltd (GEOTRACK), Report 714: Western Australia Geological Survey, S-series, S67 A2 (unpublished).

Hocking, R.M., Cockbain, A.E., 1990. Regolith. In: GSWA (Ed.), Geology and Mineral Resources of Western Australia. Western Australia Geological Survey, pp. 592–602.

Hurford, A.J., Carter, A., 1991. The role of fission track dating in discrimination of provenance. In: Morton, A.C., Todd, S.P., Haughton, P.D.W. (Eds.), Developments in Sedimentary Provenance Studies. Geological Society London Special Publication, pp. 67–78.

Hurford, A.J., Green, P.F., 1982. A user's guide to fission track dating calibration. Earth and Planetary Science Letters 59, 343–354.

Hurford, A.J., Green, P.F., 1983. The zeta age calibration of fission-track dating. Isotope Geoscience 1, 285–317.

Jablonski, D., 1997. Recent advances in the sequence stratigraphy of the Triassic to lower Cretaceous succession in the Northern Carnarvon Basin, Australia. APPEA Journal 37, 429–454.

Kinny, P.D., Nutman, A.P., Occhipinti, S.A., 2004. Reconnaissance dating of events recorded in the southern part of the Capricorn Orogen. Precambrian Research 128, 279–294.

Kohn, B.P., Weber, U.D., Raza, A., 2001. Apatite fission-track analysis of basement samples. In: Mory, A.J., Pirajno, F., Glikson, A.Y., Coker, J. (Eds.), GSWA Woodleigh 1, 2, and 2A Well Completion Report, Woodleigh Impact Structure, Southern Carnarvon Basin, Western Australia, Western Australia Geological Survey, Record 2001/6, pp. 93–96.

Kohn, B.P., Gleadow, A.J.W., Brown, R.W., Gallagher, K., O'Sullivan, P.B., Foster, D.A., 2002. Shaping the Australian crust over the last 300 million years: insights from fission track thermotectonic imaging and denudation studies of key terranes. Australian Journal of Earth Sciences 49, 697–717.

Laslett, G.M., Kendall, W.S., Gleadow, A.J.W., Duddy, I.R., 1982. Bias in measurement of fission-track length distributions. Nuclear Tracks 6 (2/3), 79–85.

Laslett, G.M., Green, P.F., Duddy, I.R., Gleadow, A.J.W., 1987. Thermal annealing of fission tracks in apatite: 2. A quantitative analysis. Chemical Geology 65, 1–13.

Le Blanc Smith, G., 1993. Geology and Permian coal resources of the Collie Basin, Western Australia. 38, Geological Survey of Western Australia, Report 38, Perth.

Li, Z.X., Powell, C.M., 2001. An outline of the palaeogeographic evolution of the Australasian region since the beginning of the Neoproterozoic. Earth Science Reviews 53, 237–277.

Libby, W.G., De Laeter, J.R., 1998. Biotite Rb–Sr age evidence for early Palaeozoic tectonism along the cratonic margin in southwestern Australia. Australian Journal of Earth Sciences 45, 623–632.

Libby, W.G., De Laeter, J.R., Armstrong, R.A., 1999. Proterozoic biotite Rb–Sr dates in the northwestern part of the Yilgarn Craton, Western Australia. Australian Journal of Earth Sciences 46, 851–860.

Martin, D.M., Thorne, A.M., 2004. Tectonic setting and basin evolution of the Bangemall Supergroup in the northwestern Capricorn Orogen. Precambrian Research 128, 385–409.

McLaren, S., Dunlap, W.J., Sandiford, M., McDougall, I., 2002. Thermochronology of high heat producing crust at Mount Painter, South Australia: implications for tectonic reactivation of continental interiors. Tectonics 21 (4), 18.

Metcalfe, I., 1988. Origin and assembley of south–east Asian continental terranes. In: Audley-Charles, M.G., Hallam, A. (Eds.), Gondwana and Tethys. Geological Society Special Publication, pp. 101–118.

Metcalfe, I., 1996. Pre-Cretaceous evolution of SE Asian terranes. In: Hall, R., Blundell, D. (Eds.), Tectonic Evolution of Southeast Asia. Geological Society Special Publication, London, pp. 97–122.

Mitchell, M.M., Kohn, B., Foster, D.A., 1998. Phanerozoic cooling in eastern South Australia: consequences for tectonic models. In: Van den Haute, P., de Corte, F. (Eds.), Advances in Fission-Track Geochronology. Kluwer Academic Publishers, Dordrecht, pp. 207–224.

Mitchell, M.M., Kohn, B., O'Sullivan, P.B., Hartley, M.J., Foster, D.A., 2002. Low-temperature thermochronology of the Mt. Painter Province, South Australia. Australian Journal of Earth Sciences 49, 551–563.

Morgan, K.H., 1993. Development, sedimentation and economic potential of palaeoriver systems of the Yilgarn Craton of Western Australia. Sedimentary Geology 85, 637–656.

Morgan, P., 2000. Heat flow. In: Veevers, J.J. (Ed.), Billion-Year Earth History of Australia and Neighbours in Gondwanaland. GEMOC Press, Sydney, pp. 82–90.

Morton, A.C., Todd, S.P., Haughton, P.D.W., 1991. Developments in sedimentary provenance studies. Geological Society Special Publications, Geological Society, London, vol. 57. 370 pp.

Mory, A.J., Iasky, R.P., 1994. Structural evolution of the onshore northern Perth Basin, Western Australia. In: Purcell, P.G., Purcell, R.R. (Eds.), The Sedimentary Basins of Western Australia: Proceedings of Petroleum Exploration Society of Australia Symposium, Perth, pp. 781–790.

Mory, A.J., Pirajno, F., Glikson, A.Y., Coker, J., 2001. GSWA Woodleigh 1, 2, and 2A well completion report, Woodleigh impact structure, Southern Carnarvon Basin, Western Australia. Western Australia Geological Survey, Record 2001/6, p. 147.

Müller, R.D., Mihut, D., Baldwin, S., 1998. A new kinematic model for the formation and evolution of the West and Northwest Australian margin. In: Purcell, P.G., Purcell, R.R. (Eds.), The Sedimentary Basins of Western Australia: Proceedings of Petroleum Exploration Society of Australia Symposium, Perth, vol. 2, pp. 55–72.

Myers, J.S., 1990. Precambrian. In: GSWA (Ed.), Geology and Mineral Resources of Western Australia. Western Australia Geological Survey, pp. 737–750.

Myers, J.S., 1993. Precambrian history of the west Australian craton and adjacent orogens. Annual reviews of Earth and Planetary Sciences 21, 453–485.

Myers, J.S., Shaw, R.D., Tyler, I.M., 1996. Tectonic evolution of Proterozoic Australia. Tectonics 15 (6), 1431–1446.

Nelson, D.R., 1995. Compilation of SHRIMP U–Pb zircon geochronology data, 1994. Geological Survey Western Australia Record 1995/3.

Nelson, D.R., 1996. Compilation of SHRIMP U–Pb zircon geochronology data, 1995. Geological Survey Western Australia Record 1996/5.

Nelson, D.R., 1997a. Evolution of the Archaean granite-greenstone terranes of the Eastern Goldfields, Western Australia: SHRIMP U–Pb zircon constraints. Precambrian Research 83, 57–81.

Nelson, D.R., 1997b. Compilation of SHRIMP U–Pb zircon geochronology data, 1996. Geological Survey Western Australia Record 1997/2.

Nelson, D.R., 1998. Compilation of SHRIMP U–Pb zircon geochronological data, 1997. Geological Survey Western Australia Record 1998/2.

Nelson, D.R., 1999. Compilation of SHRIMP U–Pb zircon geochronological data, 1998. Geological Survey Western Australia Record 1999/2.

Nelson, D.R., Myers, J.S., Nutman, A.P., 1995. Chronology and evolution of the Middle Proterozoic Albany-Fraser Orogen, Western Australia. Australian Journal of Earth Sciences 42, 481–495.

Norvick, M.S., Smith, M.A., 2001. Mapping the plate tectonic reconstruction of southern and southeastern Australia and implications for petroleum systems. Australian Petroleum Production and Exploration Association, 15–35.

Nutman, A.P., Bennett, V.C., Kinny, P.D., Price, R., 1993. Large-scale crustal structure of the northwestern Yilgarn Craton, Western Australia: evidence from Nd isotopic data and zircon geochronology. Tectonics 12 (4), 971–981.

Occhipinti, S.A., Swager, C.P., Pirajno, F., 1998. Structural-metamorphic evolution fo the Palaeoproterozoic Bryah and Padbury Groups during the Capricorn orogeny, Western Australia. Precambrian Research 90, 141–158.

Occhipinti, S.A., Sheppard, S., Passchier, C., Tyler, I.M., Nelson, D.R., 2004. Palaeoproterozoic crustal accretion and collision in the southern Capricorn Orogen: the Glenburgh Orogeny. Precambrian Research 128, 237–255.

O'Sullivan, P.B., Kohn, B., Foster, D.A., Gleadow, A.J.W., 1995. Fission track data from the Bathurst Batholith: evidence for rapid middle Cretaceous uplift and erosion within the eastern highlands of Australia. Australian Journal of Earth Sciences 42, 597–607.

Pidgeon, R.T., Cook, T.J.F., 2003. 1214 ± 5 Ma dyke from the Darling Range, southwestern Yilgarn Craton, Western Australia. Australian Journal of Earth Sciences 50, 769–773.

Pidgeon, R.T., Nemchin, A.A., 2001. 1.2 Ga mafic dyke near York, southwestern Yilgarn Craton, Western Australia. Australian Journal of Earth Sciences 48, 751–755.

Pirajno, F., Occhipinti, S.A., 2000. Three Palaeoproterozoic basins–Yerrida, Bryah and Padbury–Capricorn Orogen, Western Australia. Australian Journal of Earth Sciences 47, 675–688.

Qiu, Y., McNaughton, N.J., Groves, D.I., Dunphy, J.M., 1999. First record of 1.2 Ga quartz dioritic magmatism in the Archaean Yilgarn Craton, Western Australia, and its significance. Australian Journal of Earth Sciences 46, 421–428.

Reimold, W.U., Koeberl, C., 2000. Critical comment on: A.J. Mory et al. 'Woodleigh, Carnarvon Basin, Western Australia: a new 120 km diameter impact structure'. Earth and Planetary Science Letters 184, 353–357.

Renne, P.R., Reimold, W.U., Koeberl, C., Hough, R., Claeys, P., 2002. Comment on: "K–Ar evidence from illitic clays of a Late Devonian age for the 120 km diameter Woodleigh impact structure, Southern Carnarvon Basin, Western Australia", by I.T. Uysal, S.D. Golding, A.Y. Glikson, A.J. Mory and M. Glikson [Earth Planet. Sci. Lett. 192 (2001) 218–289]. Earth and Planetary Science Letters 201 (1), 247–252.

Sircombe, K.N., Freeman, M.J., 1999. Provenance of detrital zircons on the Western Australia coastline—implications for

the geologic history of the Perth Basin and denudation of the Yilgarn Craton. Geology 27 (10), 879–882.

Song, T., Cawood, P.A., 2000. Structural styles in the Perth Basin associated with the Mesozoic break-up of Greater India and Australia. Tectonophysics 317, 55–72.

Spikings, R.A., Foster, D.A., Kohn, B.P., Lister, G.S., 2001. Post-orogenic (<1500 Ma) thermal history of the Proterozoic Eastern Fold Belt, Mount Isa Inlier, Australia. Precambrian Research 109, 103–144.

Tewari, R.C., Veevers, J.J., 1993. Gondwana Basins of India occupy the middle of a 7500 km sector of radial valleys and lobes in central-eastern Gondwanaland. In: Findlay, R.H., Unrug, R., Banks, M.R., Veevers, J.J. (Eds.), Gondwana Eight: Assembley, Evolution and Dispersal. Proceedings of the Eighth Gondwana Symposium, Hobart, pp. 507–512.

Totterdell, J.M., Struckmeyer, H.I.M., Beynon, R.M., Bradshaw, M., Brakel, A.T., Brown, P.J., Burger, D., Cook, P.J., Jones, P.J., Langford, R.P., Mulholland, S.M., Olissoff, S., Ross, M.I., Strusz, D.L., Truswell, E.M., Walley, A.M., Wilford, G.E., Yeates, A.N., Yeung, M., Young, G.C., 1990. Australia—Evolution of a Continent. Australian Government Publishing Service, Canberra. 97 pp.

Tyler, I.M., 1990. Mafic dyke swarms. In: GSWA (Ed.), Geology and Mineral Resources of Western Australia. Western Australia Geological Survey, pp. 191–194.

Veevers, J.J., 2000. Billion-Year Earth History of Australia and Neighbours in Gondwanaland. GEMOC Press, Sydney. 388 pp.

Veevers, J.J., Saeed, E.A., Belousova, E.A., Griffin, W.L., 2005. U–Pb ages and source composition by Hf-isotope and trace-element analysis of detrital zircons in Permian sandstone and modern sands from southwestern Australia and a review of the paleogeographical and denudation history of the Yilgarn Craton. Earth-Science Reviews 68, 245–279.

Wagner, G.A., Van den Haute, P., 1992. Fission-Track Dating. Kluwer Academy. 285 pp.

Wijbrans, J.R., McDougall, I., 1987. On the metamorphic history of an Archean granitoid greenstone terrane, East Pilbara, Western Australia, using the $^{40}Ar/^{39}Ar$ age spectrum technique. Earth and Planetary Science Letters 84 (2–3), 226–242.

Wilde, S.A., Middleton, M.F., Evans, B.J., 1996. Terrane accretion in the southwestern Yilgarn Craton: evidence from a deep seismic crustal profile. Precambrian Research 78, 179–196.

Wilde, S.A., Valley, J.W., Peck, W.H., Graham, C.M., 2001. Evidence from detrital zircons for the existence of continental crust and oceans on the Earth 4.4 Gyr ago. Nature 409, 175–178.

Wingate, M.T.D., Giddings, J.W., 2000. Age and palaeomagnetism of the Mundine Well dyke swarm, Western Australia: implications for an Australia-Laurentia connection at 755 Ma. Precambrian Research 100 (1–3), 335–357.